30. Morata, G. & Kerridge, S. *Nature* **290,** 778–781 (1981).
31. Hayes, P., Sato, T. & Denell, R. *Proc. natn. Acad. Sci. U.S.A.* **87,** 545–549 (1984).
32. Struhl, G. *Nature* **308,** 454–457 (1984).
33. Sánchez-Herrero, E., Vernós, I., Marco, R. & Morata, G. *Nature* **313,** 108–113 (1985).
34. Harding, K., Wedeen, C., McGinnis, W. & Levine, M. *Science* **229,** 1236–1242 (1985).
35. Celniker, S. E., Keelan, D. J. & Lewis, E. B. *Genes Dev.* **3,** 1424–1436 (1989).
36. Lane, D. P. *et al. Proc. R. Soc.* B**226,** 25–42 (1985).
37. Biedenkapp, H., Borgmeyer, U., Sippel, A. & Klempnauer, K.-H. *Nature* **335,** 835–837 (1988).
38. Gruss, C., Wetzel, E., Baak, M., Mock, U. & Knippers, R. *Virology* **167,** 349–360 (1988).
39. Sompayrac, L. & Danna, K. *Proc. natn. Acad. Sci. U.S.A.* **87,** 3274–3278 (1990).
40. Almer, A., Rudolph, H., Hinnen, A. & Hörz, W. *EMBO J.* **5,** 2689–2696 (1986).
41. Thomas, G. H. & Elgin, S. C. R. *EMBO J.* **7,** 2191–2201 (1988).
42. Pina, B., Brüggemeier, U. & Beato, M. *Cell* **60,** 719–731 (1990).
43. Vincent, J.-P., Kassis, J. & O'Farrell, P. *EMBO J.* **9,** 2573–2578 (1990).
44. Carroll, S. B., Laymon, R. A., McCutcheon, M. A., Riley, P. D. & Scott, M. P. *Cell* **47,** 113–122 (1986).
45. Gibson, G. & Gehring, W. J. *Development* **102,** 657–675 (1988).
46. Wu, C. *Nature* **309,** 229–234 (1984).
47. Langer-Safer, P. R., Levine, M. & Ward, D. C. *Proc. natn. Acad. Sci. U.S.A.* **79,** 4381–4385 (1982).
48. Sambrook, J., Fritsch, E. F. & Maniatis, T. *Molecular Cloning, A Laboratory Manual.* 2nd edn (Cold Spring Harbor Laboratory Press, New York, 1989).
49. Tautz, D. & Pfeifle, C. *Chromosoma* **98,** 81–85 (1989).
50. Casanova, J., Sánchez-Herrero, E. & Morata, G. *Cell* **47,** 627–636 (1986).
51. DeLorenzi, M. *et al. EMBO J.* **7,** 3223–3231 (1988).

ACKNOWLEDGEMENTS. We thank D. Tautz and C. Pfeifle for communicating the whole-mount *in situ* hybridization method before publication, M. Wilcox and R. Smith for help in the early stages of this project, and M. Ashburner for advice on chromosome localizations. This work was supported by the MRC and Wellcome Trust.

LETTERS TO NATURE

The extended sodium nebula of Jupiter

Michael Mendillo, Jeffrey Baumgardner, Brian Flynn & W. Jeffrey Hughes

Department of Astronomy and Center for Space Physics, Boston University, Boston, Massachusetts 02215, USA

THE detection of a cloud of neutral sodium near Jupiter's moon Io[1] has led to the use of sodium as a tracer of processes in the jovian environment. Although relatively rare in the Io–Jupiter system, sodium atoms are easily detected because of their high efficiency for scattering sunlight at wavelengths of ~5,890 Å. Direct imaging of the sodium cloud[2] has suggested that sodium atoms are a common feature close to Io (at distances of about six Io radii, R_{Io}) and detection of high-speed sodium jets[3] suggested that sodium is present only sporadically at ~30 R_{Io} (ref. 4). Sodium emission has been reported at greater distances[5], even as far as 60 R_{Io} (ref. 6) but these observations have been controversial in view of suggestions[7] that the detection of sodium beyond ~10 R_{Io} was implausible on theoretical grounds and probably indistinguishable from terrestrial sodium airglow. Here we report on the detection of sodium to distances beyond ~400 R_J, an observation that requires the ejection rate of sodium atoms to be increased. By relating the shape of this great nebula to conditions in the plasma torus surrounding Jupiter, we show that ground-based imaging techniques can provide information about distant planetary magnetospheres.

An observational programme was initiated using a low-dispersion high-sensitivity imaging spectrograph[8] to search for emissions from ionic and neutral species at the great distances from Jupiter that would be appropriate for imaging magnetospheric structures. Our observations were made at the McDonald Observatory in Fort Davis, Texas, during the period 26 November–5 December 1989. Sodium emission was by far the strongest signal of jovian origin obtained at distances from 50 to 300 R_J, and a subsequent period of sodium-imaging observations was therefore conducted from 20 to 30 January 1990 using our standard intensified CCD detector[9] and a portable 4.2-inch aperture telescope. We obtained sodium images of 320-s exposure using a filter with a transmission of 51% and a full width at half power (FWHP) of 12 Å centred at 5,893 Å, thereby including both the D_1 (5,896 Å) and D_2 (5,890 Å) lines. Control images were taken using a filter with 60% transmission centred at 6,200 Å with a FWHP of 14 Å. Images were taken with the instrument's 6° field of view centred on Jupiter and at a point 10° north of Jupiter. We used an occulting shield and therefore did not obtain usable data in the region ±25 R_J E–W and ±13 R_J N–S.

Figure 1 gives raw data sets taken on 25 January 1990. In Fig. 1*a*, with the 5,893 Å filter on Jupiter, light contributions come from sodium in Jupiter's environment, Jupiter's light scattered by the Earth's atmosphere and within the instrument, emissions from sodium in the Earth's atmosphere, and emission from stars and terrestrial OH bands that fall in the filter's transmission curve. In Fig. 1*b*, taken with the control filter on Jupiter, light contributions come from Jupiter's scattered light, the same star field and terrestrial OH. In Fig. 1*c*, *d*, identical type images taken 10° north of Jupiter contain all of the non-jovian emissions (and a different star field).

After correcting each of the four images for instrumental effects (vignetting, bias and gain), we constructed the final image from $[(\mathrm{Na-control})_{\mathrm{Jupiter}} - (\mathrm{Na-control})_{\mathrm{Off\text{-}Jupiter}}]$, that is, (Fig. 1*a* – Fig. 1*b*) – (Fig. 1*c* – Fig. 1*d*). In addition, both of the control images were scaled to account for differences between the two filters, sensitivity of the instrument and the spectral distribution of scattered light. The resultant image, corrected for atmospheric extinction (20%) and the angular dependence of the sodium filter, is shown in Fig. 1*e*. We determined intensities using a ^{14}C source—a 3-inch diameter phosphor, illuminated uniformly by radioactively decaying carbon, that emits 80 R $Å^{-1}$ at 5,893 Å (calibrated against a tungsten halogen lamp certified by the US National Bureau of Standards).

Figure 2 shows the intensity distribution along the main axis of the nebula in Fig. 1*e*, together with an inverse-distance intensity model. Moving outward from Jupiter, the brightness levels are clearly not symmetrical, with stronger signals extending to 100 R_J on the westward side (where Io was). Intensity levels beyond 100 R_J (approximately the location of Jupiter's magnetopause) are fairly symmetrical out to ~400 R_J.

Figure 3 shows the north–south structure of the nebula at several radial distances. The coning or flaring angle in the pattern has a width of ~±22° at half-intensity. This angle is greater than the 7° tilt between Io's orbital plane (where the sodium cloud resides) and Jupiter's centrifugal equator (where the Io plasma torus densities are at their maximum). The shape of the nebula is thus not so much determined by the geometry of the interaction between the torus and the sodium cloud as by the plasma conditions and dynamics at Io's orbit, as discussed below.

We note that, as D_1 intensities are ~50% those of D_2, our intensities ($D_1 + D_2$) are a factor of ~1.5 greater than the D_2-only intensities most often quoted. The equivalent D_2 intensities from our innermost observations (50–70 R at 25 R_J) in Figs 1*e* and 2 are factors of two to three higher than those in some earlier reports of remote sodium: ~15–30 R (D_2) at 15–20 R_J (ref. 10) and ~25–30 R (D_2) at 35 R_J (ref. 5), although basically consistent with others ~30 R (D_2) at 60 R_J (ref. 6 and L. Trafton, personal communication) and ~50 R (assumed D_2) at 15–25 R_J (ref. 11). The vast extent of the nebula is revealed in the very faint (≤5 R) levels which extend to the edge of our field of view. Our calibration procedures were developed specifically for low surface brightness features and were checked as follows: terrestrial sodium levels of ~24 R (D_1 and D_2) given in Fig. 1*c* are comparable to published values[12]; use of our imaging system for H_α studies of a portion of Barnard's loop during the same January 1990 period yielded intensities in agreement with published values[13].

Owing to the strong sodium absorption feature in the solar spectrum, the relationship between intensity levels and sodium

column content along the line of sight depends on both the density and velocity structure of the nebula. Modelling studies currently underway, similar to those of other groups[10,14], suggest that fast sodium atoms ejected from the cloud near Io move along escape trajectories that are approximately tangential to co-rotation near Io ($V_r = 74$ km s^{-1} at $\sim 6\ R_J$), leading eventually to a radially streaming gas at great distances ($\geq 50\ R_J$). Assuming minimal sources and sinks beyond Io's orbit, and a constant radial velocity, yields a r^{-2} density structure. For low radial velocities ($V_r \approx 0$), the intensities in Fig. 1*e* are related to column content by $\varepsilon_r = 10^{-6}\ g\ N_T$, where ε_r is the emission in Rayleigh units at distance r in the equatorial plane, g is 0.03 photons ($D_1 + D_2$) scattered per Na atom per second, and N_T is the column content in atom cm^{-2} along the line of sight. Thus, at 100 R_J, $\varepsilon_r = 23$ R corresponds to 7.5×10^8 Na cm^{-2}. With a substantial radial velocity with respect to Jupiter (and thus to the Sun), $V_r \approx 74$ km s^{-1}, our preliminary modelling studies of the resultant spectral-line profiles suggest that the measured ε_r represents a factor of 18 enhancement over the $V_r \approx 0$ case, yielding a column content of 4.3×10^7 Na cm^{-2}. Modelling the sodium distribution along this column gives a concentration ($[Na]_r = N_T/\pi r$) of $\sim 2 \times 10^{-5}$ cm^{-3} at $r = 100\ R_J$. The flux required to maintain such a distribution with a flaring angle of $\pm\theta$ is $\Phi_{Na} = [Na]_r V_r 2\pi r(2r\theta) \approx 4 \times 10^{26}$ Na s^{-1}. Following the Brown and Schneider formalism[10] for relating the flux of fast sodium from charge exchange to the total inventory of sodium near Io, we derive a total abundance value of $\sim 8 \times 10^{31}$ atom, a factor of 80 higher than used in that model.

Our analysis thus far shows: (1) the spatial extent of sodium emission far from Jupiter is a factor of 10 larger than previously known; (2) total intensities ($D_1 + D_2$) are consistent with some earlier D_2 intensities observed in the 25-50 R_J region, yet at least a factor of two higher than others, suggesting that temporal variability may be an observable component of the nebula; (3) the fast-sodium source rate calculated from observations at 100 R_J, when interpreted in terms of standard cross-sections and model parameters[10], requires an increase in the total sodium population, or the Na^+ densities in the torus, or both (such that both multiplicative factors result in an increase by a factor of ~ 80). The most recent estimates of fluxes associated with fast sodium jets[15] are also well below (by a factor of 50) those we obtain for the nebula.

Perhaps the most surprising aspect of these observations is the well ordered shape of the sodium nebula shown in Fig. 1*e* and characterized in Fig. 3 by a flaring angle of $\sim \pm 22°$. We relate this angle to the co-rotation speed and temperature of ions in the plasma torus. Assuming that resonant charge exchange ($Na^+ + Na \rightarrow Na(fast) + Na^+$) represents the main avenue for the production of fast sodium[10], the flaring angle serves as a diagnostic of the Na^+ mean energy in the torus. If the velocity-space distribution of ions in the torus is assumed to be spherical about the co-rotation speed of ~ 74 km s^{-1}, the radius of the sphere is 74 sin 22° or ~ 28 km s^{-1}. This velocity corresponds to a sodium ion of energy 94 eV. Although Na^+ is a minor species in the torus (<5%), its thermal structure should be a tracer for the total ion population. The derived value of 94 eV is consistent with the mean ion energy of ~ 100 eV in the torus at 6 R_J reported from the 1979 Voyager encounters[16]. The strong control exerted by such magnetospheric processes on the sodium distribution far from its source results in a structure decidedly different from the gravitationally bound cloud and occasional jets of sodium long associated with Io's extended atmosphere. The fact that the shape of the structure can be used to conduct remote sensing of Jupiter's magnetospheric properties suggest a new term for such a non-spherical planetary neutral cloud, a magneto-nebula.

The ultimate fate of the sodium atoms ejected from Jupiter's magnetosphere seems to be ionization by solar extreme ultraviolet with a time constant of ~ 400 h (ref. 4). At ~ 74 km s^{-1} (or $\sim 4\ R_J\ h^{-1}$), the nebula would extend to ~ 1.5 AU in diameter

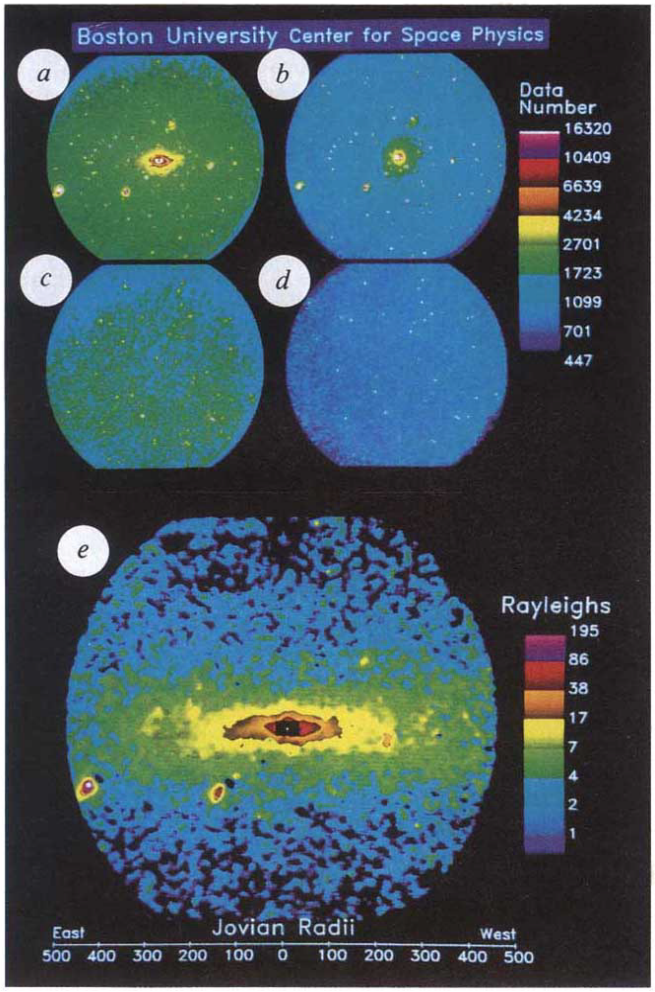

FIG. 1 Images taken on 25 January 1990 with *a*, sodium (5,893 Å) filter at 02:54:09 UT and *b*, control (6,200 Å) filter at 02:25:40 UT, both centred on Jupiter, and *c*, at 02:44:54 UT and *d*, at 02:36:43 UT with the sodium and control filters 10° north of Jupiter. A radially symmetrical pattern of scattered light is given in *b*. The terrestrial sodium brightness level from *c* was found to be ~24 R. The background through the 6,200-Å filter from *d* was ~1.5 R Å^{-1}. The brightness levels in *a*–*d* are given in original data numbers to allow for comparison. The final corrected image is shown in *e* (see text). The two bright features in the southeast quadrant are residuals from the incomplete subtraction of stars μ and η Geminorum.

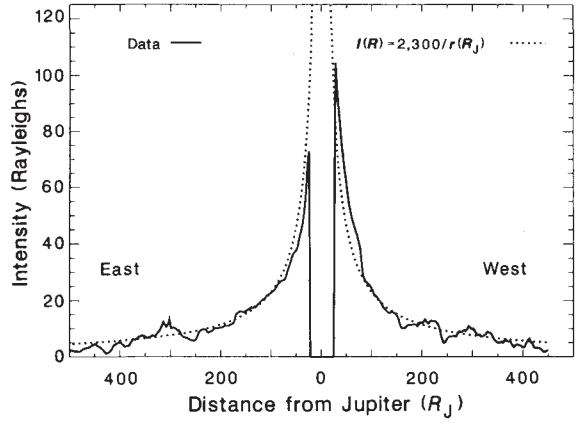

FIG. 2 Scan of the intensities in Fig. 1*e* taken along a 9-R_J-wide (5-pixel-wide) band in the equatorial plane. For comparison, an inverse-distance brightness profile is shown that is normalized to the observed values of 23 R at ±100 R_J.

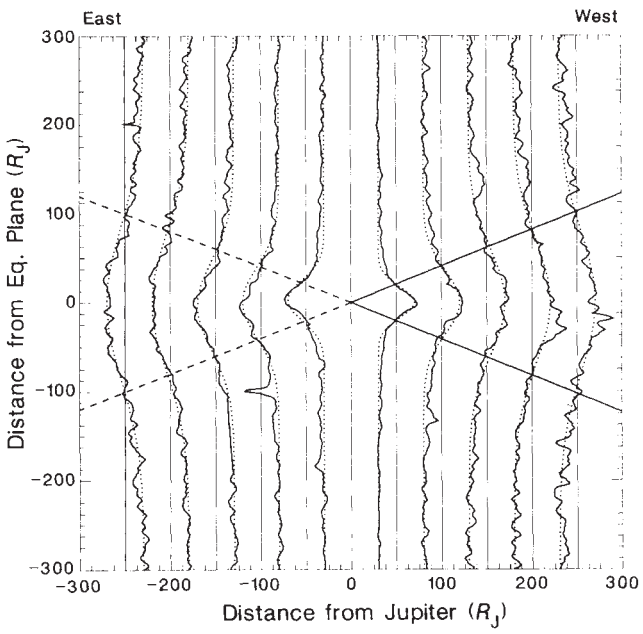

FIG. 3 Scans perpendicular to the equatorial plane at several radial distances from Jupiter. The scans have been normalized to unit intensity at the equatorial crossing point to illustrate the flaring angle defined by the half width at half maxima obtained from gaussian fits to the data (dotted curves). The western and eastern portions of the image were processed separately and resulted in nearly identical flaring angles: 22° (solid lines) and 21.3° (dashed lines). The two westernmost scans are contaminated by imperfect subtraction of light from 1 Geminorum. The small tilt of Jupiter's equatorial plane (~2°) with respect to Earth was not removed before this analysis because it has no appreciable effect on the measured half-widths.

before substantial ionization occurred. This faint cloud is perhaps the largest visible object in the Solar System, and its full extent might be detected by a space-based imaging system above the terrestrial sodium layer and scattering atmosphere. The Galileo spacecraft might also detect neutral sodium as it approaches Jupiter in 1995. Such energetic-neutral-atom imaging of magnetospheric topology has been discussed for the terrestrial and saturnian cases[17].

The mechanisms that produce Jupiter's sodium magnetonebula should also create extended clouds of the more abundant species (such as O, S, SO, SO_2). They have far weaker signatures at visible wavelengths, but might appear in space-borne ultraviolet images (the emission at 1,304 Å of O and S, for example) or in direct detections of neutral fluxes by the Galileo spacecraft. □

Received 22 May; accepted 16 October 1990.

1. Brown, R. A. in *Proc. IAU Symp.* 65, *Exploration of the Planetary Systems* (eds Woszczyk, A. & Iwaniszewska, C.) 527–531 (Reidel, Dordrecht, 1974).
2. Goldberg, B. A., Garneau, G. W. & LaVoie, S. K. *Science* **226,** 512–516 (1984).
3. Trauger, J. T. *Science* **226,** 337–341 (1984).
4. Schneider, N. M., Smyth, W. H. & McGrath, M. A. *Time-Variable Phenomena in the Jovian System, SP-494* (eds Belton, M. J. S., West, R. A. & Jurgen, R.) 75–94 (NASA, Washington, 1989).
5. Pilcher, C. B. & Schempp, W. V. *Icarus* **38,** 1–11 (1979).
6. Trafton, L. & Macy, W. Jr *Icarus* **33,** 322–325 (1978).
7. Goody, R. & Apt, J. *Planet. Space Sci.* **25,** 603–604 (1977).
8. Baumgardner, J. *Eos* **70,** 404 (1989).
9. Baumgardner, J. & Karandanis, S. *Electronic Imaging* **3,** 28–31 (1984).
10. Brown, R. A. & Schneider, N. M. *Icarus* **48,** 519–535 (1981).
11. Wehinger, P. A., Wyckoff, S. & Frohlich, A. *Icarus* **27,** 425–528 (1976).
12. Kirchhoff, V. W. J. H. *Can. J. Phys.* **64,** 1664–1672 (1986).
13. Reynolds, R. J. & Ogden, P. M. *Astrophys. J.* **229,** 942–953 (1979).
14. Pilcher, C. B., Smyth, W. H., Combi, M. R. & Fertel, J. H. *Astrophys. J.* **287,** 427–444 (1984).
15. Schneider, N. thesis, Univ. Arizona (1988).
16. Bagenal, F. in *Time-Variable Phenomena in the Jovian System, SP-494* (eds Belton, M. J. S., West, R. A. & Jurgen, R.) 196–210 (NASA, Washington, 1989).
17. Roelof, E. C. & Williams, D. J. *Johns Hopkins APL Tech. Digest* **9,** 72–76 (1990).

ACKNOWLEDGEMENTS. We thank A. Dessler, F. Bagenal, N. Schneider and G. Siscoe for discussions, E. Barker and the McDonald Observatory for support, K. Janes, R. Phelps and M. Fox for help with planning and analysis, D. Nottingham and H. Pais for assistance in the observations, S. Karandanis (Datacube Inc.) for providing digitizing hardware, and T. Mooney (Barr Assoc.) for a sodium filter. We dedicate this paper to the memory of F. Scarf.

Evidence of very-large-amplitude solitary waves in the atmosphere

Mohan K. Ramamurthy*, Brian P. Collins*, Robert M. Rauber* & Patrick C. Kennedy†

* Department of Atmospheric Sciences, University of Illinois, 105 S Gregory, Urbana, Illinois 61801, USA
† Climate and Meteorology Section, Illinois State Water Survey, Champaign, Illinois 61820, USA

ATMOSPHERIC solitary waves are gravity waves that retain their integrity over long periods because of a near balance between nonlinearity and dispersion. They have been observed on various scales in many regions of the world[1–3], but we present here detailed measurements of solitary waves with amplitudes comparable to the scale height of the lower troposphere. Two such waves were generated downstream of intense mid-tropospheric pressure troughs over the central United States. They propagated over 1,000 km (several times their wavelength) with no appreciable change in structure within a 'waveguide' formed by surface inversion and a middle tropospheric critical level. Fluctuations in surface pressure associated with the two waves exceeded 6 mbar and 10 mbar. The waves caused banded patterns of precipitation and significantly influenced other meteorological phenomena. The restoration of balance between pressure-driven air flow and the Coriolis force ('geostrophic adjustment') seems to have a prominent role in the formation of these solitary waves.

Studies have documented the existence of atmospheric solitary waves during the winter[4–7] and have revealed a large degree of similarity in the atmospheric conditions present during their initiation[8]. Several mechanisms have been proposed and documented to explain their genesis, including the hydraulic jump theory[9,10], a shearing instability mechanism[6,11,12], the geostrophic adjustment process[6,8,13], interactions of density currents with pre-existing inversions[10–14], and triggering by deep convection[2]. Although several hypotheses have been forwarded, the lack of detailed measurements through the depth of the troposphere has limited our understanding of these phenomena.

During January 1989, two large-amplitude solitary waves passed through the central United States. Throughout both events, thermodynamic and wind data were gathered at high time resolution with three instruments: a 50-MHz wind profiler[15], a 10-cm-wavelength Doppler radar[16] and a balloon-borne sounding system[17]. These measurements were made near Champaign, Illinois during an investigation of mid-latitude cyclone precipitation band structure.

The solitary waves of 5 and 14 January 1989 developed within intense wintertime mid-latitude cyclones. The waves in both cases propagated over 1,000 km before dissipating (Fig. 1). Dramatic surface pressure fluctuations were recorded at many stations. For example, the pressure dropped 10 mbar in 75 min at Cape Girardeau on 14 January, and 6 mbar over the same time period at Moline on 5 January. The arrival of the wave at many locations, as evidenced by coherent surface pressure jumps in Fig. 1, was marked by gustiness and sharp changes in the wind direction and intensity of precipitation. Narrow, very distinct precipitation bands accompanied the waves on both days (Fig. 2). The return to equilibrium pressures near pre-wave levels following wave passage (after subtracting the larger-time-scale trend) suggests that these disturbances possessed the characteristics of solitary waves rather than undular bores, where a finite pressure jump would be expected[18].

In both cases, deep pressure troughs in the middle and upper troposphere were located west of the region of solitary wave generation. In each trough, strong winds at jet-stream altitude moved northeast from the trough base into a region of reduced pressure gradient and weak winds. In such a flow pattern the ratio of the air-parcel acceleration to the Coriolis force is large,